Supplementary Materials for

A microtubule-based force-generating machinery maintains the mitotic spindle at the cell center in the early *C. elegans* embryo

Carlos Garzon-Coral[1], Horatiu A. Fantana[1], & Jonathon Howard[2]*

correspondence to: jonathon.howard@yale.edu

This PDF file includes:

Materials and Methods
Supplementary Text
Figs. S1 to S14
Tables S1 to S2
Captions for Movies S1 to S5

Other Supplementary Materials for this manuscript includes the following:

Movies S1 to S5

Materials and Methods

Magnetic tweezers

The two probes of the magnetic tweezers were superparamagnetic rods 6 mm in diameter and 120 mm long. One was made of MuMetall (Vacuumschmelze GmbH, Hanau) and the other HyMu-80 (Carpenter Technology, Reading, PA). The respective probes were sharpened at one end to angles of 35° and 45°. Each probe was polished to eliminate small surface imperfections and then annealed to increase the permeability of the material. To induce a magnetic gradient, a current of 0.2 to 1 A was applied to a solenoid made of 0.5 mm diameter copper wire wrapped 350 times around the rods using a Teflon support (*1*). The solenoids were connected to a custom-built voltage-controlled current source, which was controlled using a DAQ card (PCI-MIO-16E-4, National Instruments, Munich). The magnetic probes were mounted on an AxioVert 200M inverted microscope (Zeiss, Jena) and positioned by InjectMan NI2 micromanipulators (Eppendorf). A permanent magnet (termed the z-pole) connected to a sharp tip made of MuMetall was mounted on the nosepiece and could be swung in to replace the objective to bring the bead down towards the bottom of the chamber. For more details see Fig. S1A.

The inverted microscope was equipped with DIC optics, fluorescence filters (filter sets F46-002 for eGFP and F46-008 for Texas-Red, AHF analysentechnik) and two cameras, a back-illuminated Andor iXon+ 897 EMCCD camera (512 x 512 pixels, 14-bit) and an Andor Luca R camera (1004 x 1002 pixels, 14-bit). The objective was a 63x/1.2 water immersion C-Apochromat (Zeiss). Image data were streamed directly to a fast hard drive (10000 rpm, Western Digital) at 10-31 fps. The magnetic tweezers setup was controlled using LabVIEW (National Instruments).

Force Calibration

Because magnetic fields pass virtually unaltered through cells due to the negligible susceptibility of biological materials, force calibrations done inside open PDMS chambers should apply inside the embryos. Force-distance curves were obtained by tracking the position of 1.0 μm (1.04 ± 0.02 μm, mean ± SD, Fig. S1B) superparamagnetic beads (MyOne, Life Technologies) as they moved through mineral oil (viscosity = 1050 mPa·s, Brookfield, Middleboro, MA, Fig. S1C) toward the magnetic poles after a current of 0.2 to 1.0 A was applied to the solenoid. The force calibration was performed as follows: One magnetic pole was placed 50-100 μm away from an isolated bead, which was more than 100 μm away from any surface to avoid surface interactions. After flows in the chamber died down, the current was turned on and the position of the fluorescent bead was imaged (Fig. S1) and tracked using FIESTA(*2*). The forces acting on the bead were calculated using Stokes' law, and force-distance curves were generated (Fig. S1D). To characterise the force, a sum of two exponential functions (

$F(x) = A\exp(-x/a) + B\exp(-x/b)$) was fitted to the mean force-distance curves. The parameters of this function (A, B, a and b) were calculated and saved for the range of applied currents and then used to calculate the force during the experiments.

The beads were coated with 750 Da mPEG (Rapp Polymere,Tuebingen) and Alexa Fluor 488 (Life Technologies) and injected directly into the distal gonad of adult *C. elegans* worms using microneedles pulled from 1.0 mm diameter glass capillaries (GC100TF-10, Harvard Apparatus, Holliston) using a P-97 micropipette puller (Sutter Instruments). The mPEG minimizes non-specific binding to cellular or gonadal structures, and the Alexa dye facilitates the simultaneous tracking of the beads and the centrosomes inside the embryo by fluorescence microscopy. Because the gonadal cytoplasm is continually packaged into maturing oocytes (*3*), a fraction of the injected beads were later incorporated into the oocytes, which were then fertilized and became embryos (*4*). Worms were dissected in egg salts (0.1 M NaCl, 4% sucrose) using a stereomicroscope 2 - 6 h post-injection at 22 °C. Single embryos harvested before or during pronuclear meeting were transferred using a mouth pipette to an experimental chamber. The cover-glass was coated with a 1 mm diameter patch of Cell Tak (BD Biosciences) freshly cured with ethanol (Fig. 1a). The embryo adhered to the patch and was covered with a 50 - 100 µl drop of EB buffer (10 mM Tris-Cl, pH 8.5, Qiagen). The chamber was mounted on a revolvable sample holder on the magnetic tweezer set-up (Fig. S1A).

Force experiments

To determine how the metaphase spindle moves in response to the external forces, we used fluorescence microscopy to visualize simultaneously the beads, the two poles of the spindle (using GFP-labeled g-tubulin to label the centrosome) and the chromatin (GFP-labeled histone HA1 to label the nucleosomes). A bead was positioned next to the centrosome of a dividing cell as follows. First, the bead was first brought into the plane of the spindle plane: if the bead was below the plane, the magnetic poles were used to move it up (the magnetic force has a strong upward component when the magnetic probes are more than 50 µm above the cover slide); if the bead was above the plane, the z-pole was used to move it down. Once the bead was in the spindle plane, the bead was brought next to a centrosome using several 0.1 - 1 second force pulses. The microtubule array radiating from the spindle pole guided the incoming bead towards the centrosome and stabilized it. This procedure permitted the application of force to the centrosome without specific attachment.

The embryo was aligned such that the line from the bead to the axis of the magnetic pole passing by the centrosome position was perpendicular to the transverse axis of the embryo (Fig. 1a). During an experiment, a single electromagnetic pole was used and the z-pole and the other electromagnetic pole were withdrawn more than 30 mm and 60 mm respectively away from the embryo.

We focused initially on metaphase during which there was a time window of about one half a minute when the spindle was aligned along the anterior-posterior (AP) axis (30.1 ± 27.1 s, n = 45, mean ± SD). Outside this window, the spindle was moving: prior to metaphase, there was a dramatic translocation of the pronuclei centrosome complex (PCC, (*5*, *6*)) that initially centers and orients the spindle; at the end of metaphase and during early-to-mid anaphase, the spindle underwent a large-amplitude rocking motion as it elongated and moved towards the posterior end of the embryo (*5*, *7*). Thus, during metaphase the position was stable enough to make mechanical measurements.

The experiments were mostly done on the anterior pole of the spindle. The metaphase experiments were performed on embryos that had a fully formed metaphase plate and whose spindle was at the cell center. Recordings where spindle oscillations were evident during metaphase or late anaphase (for the control anaphase embryos) were discarded. The experiments during anaphase were performed on the anterior pole of the single-cell embryos, and in control embryos on the anterior pole after oscillations died out. The anaphase experiments in the *gpr-1/2* (RNAi) embryos were performed on the anterior pole once anaphase onset occurred. The force experiments were run at 10 fps but note that in the Fig. 2 and Fig. 3 only every third data point is displayed for clarity. The complete set of data points of Fig. 2 is displayed in Fig. S13.

Once aligned, force pulses of 20 to 60 pN during metaphase and 20 to 200 pN during anaphase, and 5 to 20 second durations were applied to the centrosome with 10 to 50 seconds relaxation periods in between. The bead-centrosome contact was confirmed using two parameters: a constant bead-centrosome distance of about 2 μm (2.01 ± 0.09 μm, mean ± SE, n = 34) in metaphase (Figure S4) and 2.2 μm (2.19 ± 0.09 μm, mean ± SE, n = 13) in anaphase; and a deceleration of the bead near the centrosome when the force pulse was applied (Figure S4). In some experiments the bead escaped the microtubule array during the force pulse (see third force pulse of Fig. 1, Fig. S4 and Movie S1). For the experiments where the bead escaped, the microtubule array only the initial part of centrosome displacement (when the bead and the centrosome were in the same focal plane) was used in the analysis. After the experiment, some embryos were transferred to feeding plates to confirm that they hatched and developed into fertile adults (Fig. S2).

We observed that the bead-centrosome distance often reached a plateau (see second force pulse in Fig. S4) on average 1 second after the bead make contact with the centrosome (Fig. S4C). We note that the centrosome began its displacement before the bead-centrosome distance reached the plateau. Thus, we argue that the force applied using magnetic beads begins to be transmitted to the spindle once a minimal distance bead-centrosome is reached (2.5 ± 0.1 μm, initial contact). The force is transmitted almost completely to the spindle soon after the initial contact when the distance bead-centrosome reaches a plateau (bead-centrosome distance of 2 μm, Fig. S4 and Fig. 1B

panel c). Only experiments where the bead and the centrosome remained in the same optical plane were used in the analysis. We found that the structural integrity of the centrosome and the spindle was sufficient to resist forces of hundreds of pN exerted by one or more 1 μm beads: forces up to 650 pN were applied to the centrosome without compromising the structural integrity of the centrosome. Therefore, the centrosomes and the microtubules that surrounded it provided a robust handle to transmit the external force to the spindle.

Image analysis

During the force pulses, the position of the centrosome and the magnetic bead were tracked using software written in MATLAB (The MathWorks, Inc., Natick). A model with two symmetrical Gaussians and a parabolic-tilted background was fit to the signal coming from the γ-tubulin::GFP of the centrosome, the fluorescent signal from the bead, and the background signal from the embryo. The equation used was:

$$I(x,y) = I_c exp\left[\frac{(x-x_c)^2}{2\sigma_c^2}\right] + I_b exp\left[\frac{(x-x_b)^2}{2\sigma_b^2}\right] + ax^2 + \mathrm{bx} + \mathrm{mx} + \mathrm{I} \quad \text{Eq. (1)}$$

where (x_c,y_c) and (x_b,y_b) are the coordinates of the centrosome and bead respectively; σ_c^2 and σ_b^2 are the variances of the centrosome and bead respectively; $ax^2 + bx$ defines the parabolic shape of the background intensity along the transverse axis; and $my + I$ defines the tilted background of the intensity along the A-P axis. For details see Fig. S3.

Motion analysis and modeling

The centering mechanism was described by the creeping response of a Voigt viscoelastic element (damped spring model):

$$\frac{x(t)}{F(t)} = \frac{1}{k}\left[1 - \exp\left(-t\frac{\kappa}{\gamma}\right)\right] \quad \text{Eq. (2)}$$

F(t) is the force, which changed to a small extent as the bead-probe distance changed during the experiment. To calculate the spring constant (κ) and the drag coefficient (γ), the mean displacement of the centrosome (blue dots in Fig. 2a) was fit to Eq. (2) using a non-linear regression weighted by the SE for each data point (red bars in Fig. 2a). The time constant (τ) was calculated as the ratio of the drag coefficient and the spring constant (γ/κ).

To calculate the relaxation time constants, the mean relaxation displacement data were scaled to the maximum displacement (black dots in Fig. 2b). These data were then fit to the creep relaxation equation of a damped spring,

$$\frac{x(t)}{x(0)} = A\left[\exp\left(\frac{-t}{\tau}\right)\right] \quad \text{Eq. (3)}$$

using a non-linear regression.

We found that the values of the spring constant, drag coefficient and characteristic times were not statistically different when (i) they were calculated on the average values

of the fits of the individual traces; (ii) the fit to the average of the individual traces; (iii) they were obtained by bootstrap (Table 1). The SEs were calculated using bootstrap. The 95% confidence intervals were reported when the distributions obtained from bootstrap were not symmetric (*8*, *9*).

Mechanical properties of the cytoplasm

Some 1.0 μm beads (Dynalbeads, Life Technologies) were dragged in the cytoplasm parallel to the transverse axis of the embryo. The beads were placed in the middle of the embryo along the *z*-axis using the z-pole and in the anterior part of the embryo using the electromagnetic poles during pronuclear meeting. In this region the density of microtubules growing out from the spindle is low (*10*). The beads were dragged with forces of 1 to 20 pN applied for 0.3 to 1 seconds with 5 to 9 seconds in between force application (Fig. S6A). Movies were taken at 31 fps, and the position of the bead was tracked using MATLAB. We computed the bead position during the rising phase of the beads in the cytoplasm scaled by the applied force (Fig S6C) as explained above for the movement of the spindle. We fitted a Voigt (Eq. (2)) and a D-S-Voigt element to the data (Eq. (4)) (Fig S6C)

$$\frac{x(t)}{F(t)} = \frac{1}{\kappa}\left[1 - exp\left(-t\frac{k}{\gamma_1}\right)\right] + \frac{t}{\gamma_2} \qquad \text{Eq. (4)}$$

We found that the D-S-Voigt element describes well the rising movement of beads in the cytoplasm (Fig. S6C) and provides a better fit than the Voigt element (F-test: $P<0.00001$). The bead position during the relaxation phase was normalized by the initial position and the base line was subtracted (Fig. S6D). The traces were fit with the Eq. (3).

Strains, RNAi protocol

Worms (TH30 strain, γ-tubulin::GFP; histone::GFP, Hyman Lab, MPI-CBG) were grown at 22°C. RNAi by feeding was performed according to (*11*). Briefly, L2 to L4 synchronized larvae were grown on RNAi feeding plates for at least 48 hours before injection and they were incubated on RNAi feeding plates for 3 to 4 hours before dissection. To generate *gpr-1/2+fzy-1 (RNAi)* embryos, L2 worms were incubated on *gpr-1/2* RNAi plates for 36 hours, and then were grown overnight on *gpr-1/2+fzy-1* RNAi plates, with a 3:1 ratio. The RNAi Sequence IDs used in this study are shown in Supplementary Table 1.

Quantification of microtubules ends

The imaging of microtubules ends at the cortex was done as described in (*12*). EB2::GFP worms were grown at 25 °C (TH66, Hyman Lab, MPI-CBG). The embryos were mounted in agar pads between two cover slides and carefully positioned on the microscope to minimize shape changes. The imaging was done under a spinning disk microscope: Zeiss inverted microscope 200M equipped with a Digital CMOS camera ORCA Flash4.0 V2: C11440- 22CU and a 63x (1.3 NA) water immersion objective

(Zeiss, Jena). The cortex was imaged for less than 135 frames at 5 fps. The images were corrected for photobleaching using the histogram matching method from FIJI. The tracks of microtubules ends were extracted using FIESTA(*2*) and then analyzed using MATLAB. The average values of the characteristic times and lengths of the tracks were calculated using an exponential fit ($y(x) = A\exp(-x/a)$ where $a = \tau$ or $a = l$), to the individual data points weighted by the SE. The fit values are presented as mean ± 95% confidence intervals.

Quantification of the time the spindle spends at the cell center

To determine the time the spindle remained at the cell center, embryos expressing fluorescent markers for the centrosomes and chromosomes (TH30 strain, γ-tubulin::GFP; histone::GFP, Hyman Lab, MPI-CBG) were imaged during mitosis at 10 fps using an iXon+ 897 EMCCD camera. The spindle was considered to be at the center of the cell if both centrosomes were less than 2.5% of the cell's width from the AP axis, and the metaphase plate was less than 2.5% of the cell's length from the midpoint of the AP axis (Fig. S9). The dimensions and orientation of the axis of the embryo were determined by fitting an ellipse to the perimeter using the cytoplasmic fluorescence.

PH::GFP (TH155, Hyman Lab, MPI-CBG) was used to visualize the membrane of the *C. elegans* embryos (*13*), and the cell's contour was computed using KoreTechs (Fig. S8C) (*14*). The Imaging was done with a spinning disk microscope: Zeiss inverted microscope 200M equipped with a Digital CMOS camera ORCA Flash4.0 V2: C11440-22CU and a 63x (1.3 NA) water immersion objective (Zeiss, Jena) at 1 frame per second for the complete cell division. The values for a 2D ellipse (long axis and short axis) were used to estimate the volume and surface of a 3D ellipsoid assuming the embryo is radially symmetric around the AP axis. The long and short axes of the *C. elegans* embryos were calculated to be 50.8 ± 2.8 μm and 35.2 ± 1.1 μm (mean ± SD) respectively (Fig. S8). The *C. elegans* embryos maintained their shape and dimension during metaphase. The total cell surface area and volume during metaphase were 5,500 ± 700 μm^2 and the volume of 37,000 ± 7,000 um^3 (mean ± SD, $n = 7$) respectively (Fig. S8E).

Taking into account the density of microtubules (Fig S11) and the cortical area, we estimated that on average 120 ± 9 (mean ± SE, $n = 10$) microtubules are in contact at the cortex per spindle pole at any given point of time. Because we only considered microtubules that stayed longer than 2 frames (400 ms) in the analysis, this number is an underestimate. We estimate that the total number of microtubules in contact to the cortex per spindle pole at any point in time is 210 ± 16 after correction for the missed events.

Supplementary Text

Drag coefficient

The cortical pushing model (*15*) predicts that a dynamic array of microtubules that is confined between two boundaries (i.e. the cortex) will experience a drag force. This force arises as follows: when the array moves towards one cortex, the arrival of microtubules to that cortex is enhanced because the arrays velocity augments the microtubules' growth velocity. At the other cortex, the arrival rate increases. Thus the relative number of pushing microtubules increases at the cortex towards which the array is moving. The increase in cortical microtubule number leads to a force which increase with the speed. This is an effective drag force, the centering drag.

The magnitude of the drag coefficient is $\Gamma \approx M\, f_E / v^+$ (*15*), where, Γ is the drag coefficient, M is the number of microtubules in contact with the cortex, f_E is the buckling force (≈1 pN for a 15 μm long microtubule (*16*, *17*)) and v^+ is the growth velocity of microtubules in the cytoplasm (≈ 0.8 μm/s (*18*) and see Fig. S11E). Using these parameter values and M = 200 from the text, we obtain a drag coefficient of ≈250 pNs/μm, which is within a factor of two of the measured value. We consider this to be cl;ose given that the model is 1D. Thus, the cortical pushing model is consistent with the experiments. That *klp-7* (RNAi) embryos and embryos during anaphase have higher drag coefficients is also in agreement with the cortical pushing model as the number of microtubules is increased. Thus, the drag coefficient values we found are consistent with a model in which the polymerization forces of microtubules are responsible for centering.

Kinetics of spindle relaxation

During the force experiments, we noted that the spindle appeared to relax following force cessation at a slower rate than it climbed following force onset. This behavior was seen under several different experimental conditions (Table 1). For any linear model, the rising and falling time constants are expected to be the same. While it is possible that the different rates (which were obtained from single-exponential fits) are due to inherent non-linearities such as microtubule buckling, load-dependent catastrophe or a shadowing effect by the bead of microtubules growing in that direction. For example, if we fit to a model with two exponentials, corresponding to two processes occurring in parallel with different rate constants, then we can simultaneously fit both the rising and relaxation phases with a single parameter set (Fig. S13). Such a slower phase is difficult to rule out because of the limited duration of the force steps, which in turn are limited by the relatively short quiescent time the spindles remain at the cell center (Fig. S9). Thus, although non-linearities could explain our data, we cannot exclude linear models.

Negative stiffness due to cortical pulling force generators.

We found that in metaphase the centering stiffness increased in *gpr-1/2* (RNAi) embryos. This shows that the cortical force generators are not an essential component of the centering stiffness, and suggests that the cortical force generators may contribute a negative stiffness (*7*, *15*). Cortical force generators pulling on microtubules are expected to generate a negative stiffness: this arises because when the spindle moves away from

the center, more force generators engage with the ends of astral microtubules on the closer side. This leads to a force imbalance that continues to move the aster in that direction away from the center (*15*). If the cortical force generators generate a negative stiffness, then GPR-1/2 by RNAi, should increase the apparent stiffness of the centering machinery (the net stiffness would be the sum of the positive and negative contributions)

We found that in anaphase the centering stiffness increased in *gpr-1/2* (RNAi) embryos, though the increase was not statistically significant at the 95% level. Observing a significant change is made difficult by the high value of the stiffness and the associated increase in uncertainty.

It is important to note that the *gpr-1/2* experiments were done throughout anaphase while the controls were done in late anaphase (following oscillation die-down). When the GPR1/2 anaphase data is splitting it into early, mid and late anaphase, we found a trend that the stiffness increases over anaphase, but it is not significant at the 95% confidence level (Supplementary Table S2). Thus, the idea that the cortical force generators are anti-centering elements is consistent with our anaphase data (in addition to the metaphase data).

Centrosome fragmentation experiments

In earlier work, Grill et al (2003) (*20*) and Labbe et al. (2004) (*19*) reported that upon laser ablation, the centrosomal fragments move towards the cortex, which suggests the centrosome is being pulled rather than pushed. We do not believe that these results contradict the current findings. There are two main arguments to reconcile the Grill et al. and Labbe et al. results with the present results. The first is that before laser ablation, it is expected that the opposing pulling forces on the centrosome from the cortical force generators will for the most part cancel. When the centrosome is fragmented, the forces no longer cancel and the pulling fragments overwhelm the opposing pushing forces and move towards the cortex. Thus fragmentation may preferentially make the pulling forces more evident. The second argument is subtler: laser ablation may actually increase the strength of the cortical pulling forces. This follows from the Pecreaux et al. 2006 (*7*) model in which it is proposed that the oscillations during transverse oscillations (when the Grill et al. experiments are done) are due to load-dependent detachment of the cortical force generators. If this is correct, then when the centrosome is fragmented, the load on the motors (from the cortex on the opposite side) is reduced, increasing the fraction of active motors and increasing the net force from the cortical force generators. This is expected to augment the fragmentation process. Finally, the fragments do not move all the way to the cortex, but rather stop after a 2-3 microns (during metaphase, Labbe et al. 2004). This shows that there must be an opposing force, which we believe is the centering force that we have identified (and likely due to pushing of microtubules against the cortex that are still able to nucleate from the centrosome fragments (*19*)).

Thus, we do not believe that our results contradict Grill et al. 2003 or Labbe et al.

2004, but rather show that two different forces acts simultaneously on the spindle to accomplish cell function; while the centering force (namely microtubule pushing) leads to centering, the cortical pulling forces shifts the position of the spindle towards the posterior of the embryo during late metaphase and anaphase. In the absence of a centering force, which counteracts the cortical pulling forces, centering is affected. This may be observed when cortical pulling forces are too strong and overwrite the centering force (*21*). Thus, cortical pulling forces and cortical pushing forces may act simultaneously to accomplish spindle positioning.

References

1. P. Kollmannsberger, B. Fabry, *Rev. Sci. Instrum.* **78**, 114301 (2007).
2. F. Ruhnow, D. Zwicker, S. Diez, **100**, 2820–2828 (2011).
3. U. Wolke, E. A. Jezuit, J. R. Priess, *Development* **134**, 2227–2236 (2007).
4. B. R. Daniels, E. M. Perkins, T. M. Dobrowsky, S. X. Sun, D. Wirtz, *J Cell Biol* **184**, 473–479 (2009).
5. C. R. Cowan, A. A. Hyman, **20**, 427–453 (2004).
6. M. Galli, S. Van Den Heuvel, *Annu. Rev. Genet.* **42**, 389–411 (2008).
7. J. Pecreaux *et al.*, *Current Biology* **16**, 2111–2122 (2006).
8. B. Efron, R. Tibshirani, *Statistical Science* **1**, 54–75 (1986).
9. T. J. DiCiccio, B. Efron, *Statistical Science* **11**, 189–228 (1996).
10. A. A. Hyman, J. G. White, *J Cell Biol* **105**, 2123–2135 (1987).
11. R. S. Kamath, M. Martinez-Campos, P. Zipperlen, A. G. Fraser, J. Ahringer, *Genome Biol* **2**, (2001).
12. C. Kozlowski, M. Srayko, F. Nedelec, *Cell* **129**, 499–510 (2007).
13. S. Redemann *et al.*, *PLoS ONE* **5**, e12301 (2010).
14. M. Biro *et al.*, *Cytoskeleton* **70**, 741–754 (2013).
15. J. Howard, *Phys Biol* **3**, 54–66 (2006).
16. F. Gittes, B. Mickey, J. Nettleton, J. Howard, *J Cell Biol* **120**, 923–934 (1993).
17. M. Dogterom, B. Yurke, *Science* **278**, 856–860 (1997).
18. M. Srayko, A. Kaya, J. Stamford, A. A. Hyman, *Dev Cell* **9**, 223–236 (2005).
19. J.-C. Labbé, E. K. McCarthy, B. Goldstein, *J Cell Biol* **167**, 245–256 (2004).
20. S. W. Grill, J. Howard, E. Schäffer, E. H. K. Stelzer, A. A. Hyman, *Science* **301**, 518–521 (2003).
21. S. Redemann *et al.*, *Nat Methods* **8**, 250–252 (2011).

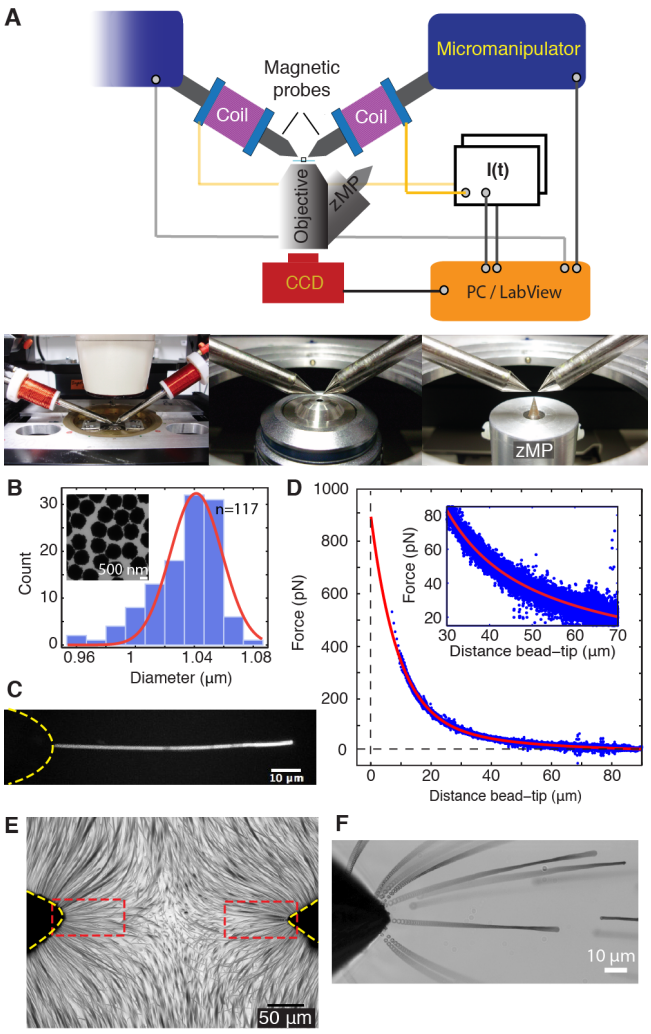

Fig. S1.

Magnetic tweezers set-up and force calibration. (A) Diagram (upper) and photos (lower) of the magnetic tweezers set-up. Two magnetic probes are positioned over the stage, which is equipped with a rotating specimen holder. The *z* magnetic probe (zMP) can be brought under the sample using the microscope's nose-piece. **(B)** Histogram of the diameters of the 1-µm-diameter MyOne superparamagnetic beads (Dynalbeads, Life Technologies) imaged by electron microscopy (inset). **(C)** Maximum projection image of a bead coated with 750 Da mPEG (Rapp Polymere) and Alexa Fluor 488 moving in 1050 mPas mineral oil along the magnetic field gradient produced by the magnetic probe (yellow broken line). **(D)** Force-distance calibration curve (double exponential fit in red, see Methods) calculated from 15 independent experiments (blue), each corresponding to a single bead moving towards the magnetic probe as shown in C. Inset shows the force for the bead-tip distances normally used during the experiments. The applied current was 1.0 A. **(E)** Maximum-projection image of 1-µm beads moving towards the magnetic probes. At shallow angles close to the probe tips (shown in the regions bounded by the red broken lines), the movement of the bead is almost linear. The experiments and the calibrations were done all were done within this region. **(F)** Close up of 1-µm beads moving towards the magnetic probe.

Fig. S2
Internalized beads in embryos. An embryo containing a 1.0-μm magnetic bead (arrowhead) was incubated on a NGM plate (left). It developed into a young larva (right); the inset shows a magnified image of the bead (arrowhead) in the body of the larva.

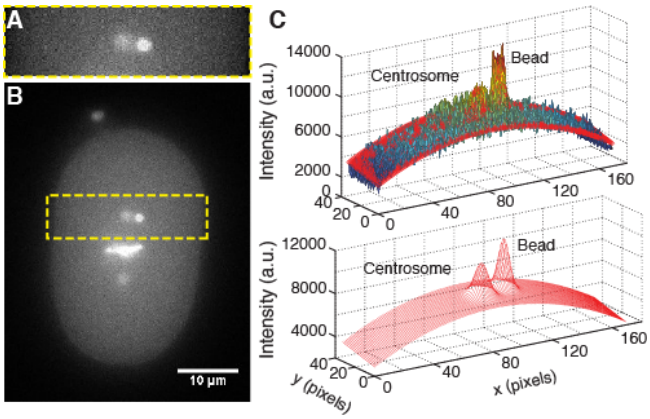

Fig. S3

Tracking the centrosome and the bead. (A) Region of interest outlined in B. **(B)** Initial frame where the bead came in contact with the centrosome during the experiment of Fig. 1B. (**C**) The intensity data (upper) were fit to the model (Eq. 1 in the methods, lower).

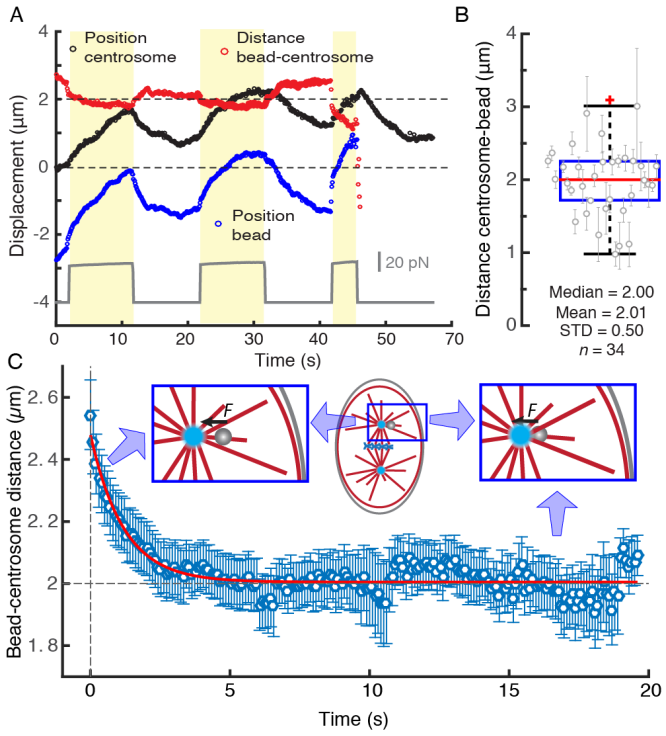

Fig. S4

Bead-centrosome distance. (A) Tracks of bead (blue) and the centrosome (black) in the experiment shown in Fig. 1. The bead-centrosome distance is shown in red. **(B)** Box plot of the bead-centrosome distance in the experiments of Fig. 2. The mean and the standard deviation of every bead-centrosome trace are shown in gray. **(C)** Mean behavior of the bead-centrosome distance over time. Error bars are SEs. The solid red line shows and exponential fit to the data (τ = 1.0 ± 0.1 s). The inset shows a model for the nestling of the bead into the microtubule array.

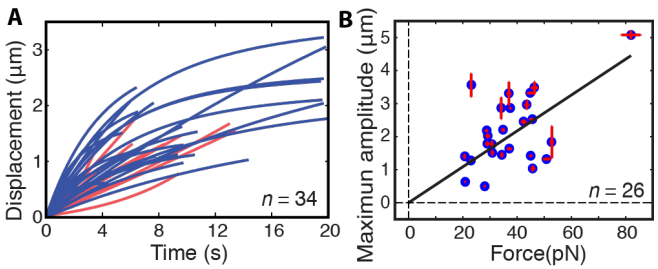

Fig. S5

Compliance associated with centering. (A) Fits of the damped spring model to individual displacement traces. Of the 34 traces used in the average response in the text (Fig. 1), fits to individual traces converge only in 26 traces (dark blue). The fits of the traces, which failed to converge, are shown in red. **(B)** For each blue trace in **A**, the estimated maximum amplitude from the curve fit (x_{max}) is plotted against the average applied force. Error bars denote the SD of the force and the 95% confidence interval of the maximum amplitude from the fit.

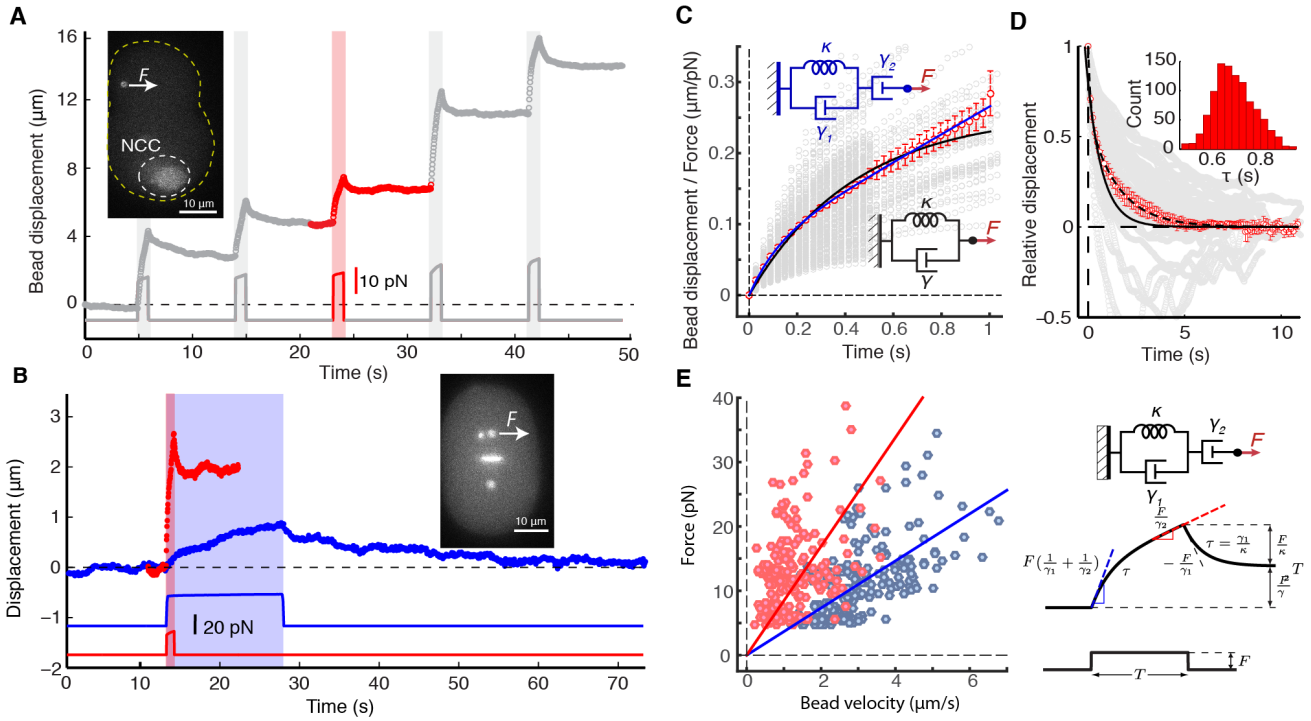

Fig. S6

Viscoelastic forces acting on beads in the cytoplasm. (A) Response of a bead to brief force steps in the cytoplasm far from the nuclear centrosome complex (NCC). The bead location before the experiment is shown in the inset image. See movie S2. **(B)** The red trace is from A and the blue trace is the response of a spindle during metaphase in a *gpr-1/2/fzy-1 (RNAi)* embryo (see movie S5). Right-upper inset shows the frame when the bead first made contact with the spindle pole; arrow shows the direction of the force. Scale bar 10 μm. Note that the bead in the cytoplasm responds much more quickly than when is embedded in the spindle. The relaxation following force cessation is incomplete. **(C)** The average movement of beads in the cytoplasm. The circles and error bars represent the average and standard error respectively. The black solid line shows a fit to a Voigt element (κ = 5.3 ± 0.2 pN/μm, γ = 1.5 ± 0.1 pN·s/μm and τ = 0.28 ± 0.02 s). The solid blue line represents the fit to a D-S-Voigt element (κ = 14.5 ± 2.2 pN/μm, γ_1 = 1.7 ± 0.1 pN·s/μm (τ = 0.12 ± 0.02 s) and γ_2 = 5.3 ± 1.3 pN·s/μm). The insets show the Voig element (black) and the D-S-Voigt element (blue). Raw data is presented in gray and smoothed using an 11 points window (n = 212) **(D)** Relaxation of beads in the cytoplasm. Curve denotes the mean and error bars denote the SE. Solid black line is a non-linear fit to a single exponential; τ = 0.76 ± 0.03, mean ± SE. SE calculated from bootstrap, see table 1). Broken line is a non-linear fit to a double exponential ($x(t) = A\exp(-t/\tau_1) + B\exp(-t/\tau_2)$; τ_1=0.12 ± 0.01 and τ_2=1.53 ± 0.03). Raw data is presented in gray and smoothed using an 11 point window (n = 115). Inset shows the histogram of the characteristic time (single exponential fits) obtained from bootstrapping the individual curves. **(E)** Force-velocity relation of beads in the cytoplasm (left) for the initial phase of

the movement (blue) and for the second phase (red) indicated in the simulated trace (right). The solid lines are linear fits through the origin. The slopes are 1.8 ± 0.1 pN·s/μm (blue) and 4.2 ± 0.4 pN·s/μm (red).

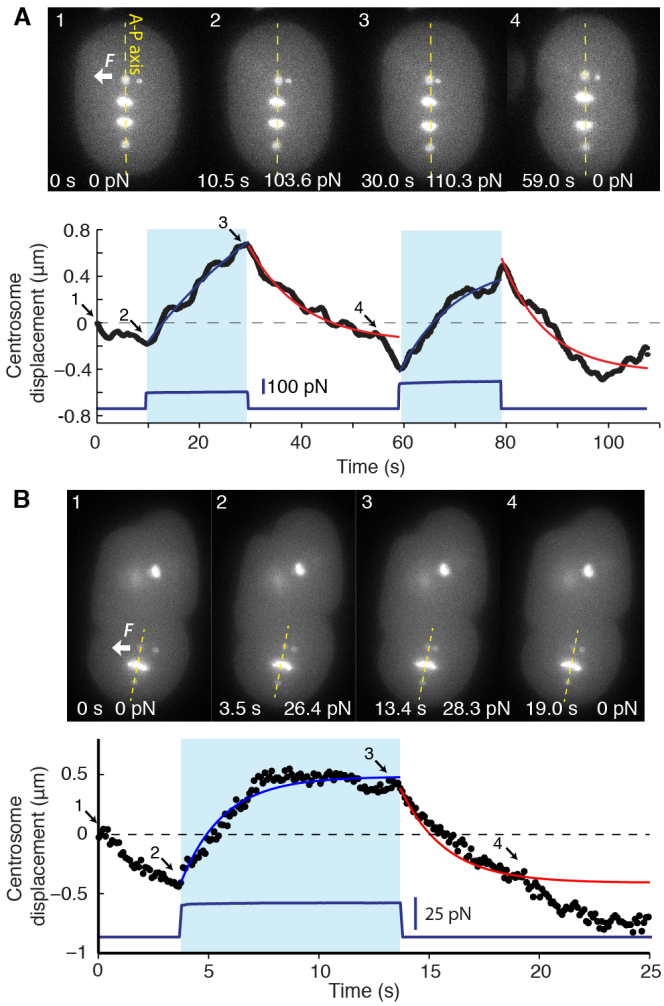

Fig. S7

Force experiments in P1 and anaphase cells. (A) Images from a video of the displacement of the spindle during anaphase (upper). Times and forces are indicated on each frame. Tracking of the centrosome (lower). The numbers indicate the times when the images above were taken. **(B)** Images from a video of the displacement of the spindle in a P1 cell (upper). Times and forces are indicated on each frame. Tracking of the centrosome (lower). The first image corresponds to $t = 0$. The spindle axis is used as a baseline (dashed line).

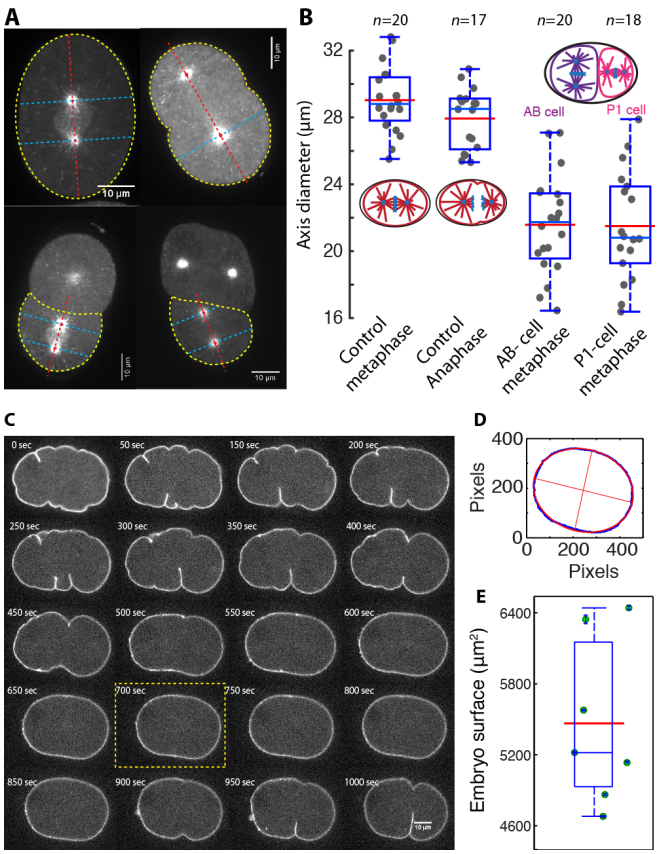

Fig. S8

Axis length in the one- and two-cell embryos. (A) The axis length at the location of the spindle pole was determined by the distance between opposite sides of the cortex along a line perpendicular to the A-P axis in the control metaphase embryos (left-top) or by the axis formed by the two spindle poles during anaphase (right-top) and in P1 cells (bottom). **(B)** Boxplot of axis lengths for one- and two-cell embryos. Red line denotes the mean**. (C)** PH::GFP signal during cell division of a single-cell *C. elegans* embryo. $t = 0$ s denotes the onset of cortical ruffles. **(D)** Ellipse fit to the contour extracted from the image in C bounded by the yellow broken line. **(E)** Boxplot of the surface estimated from 6 embryos during metaphase. Red line denotes the mean.

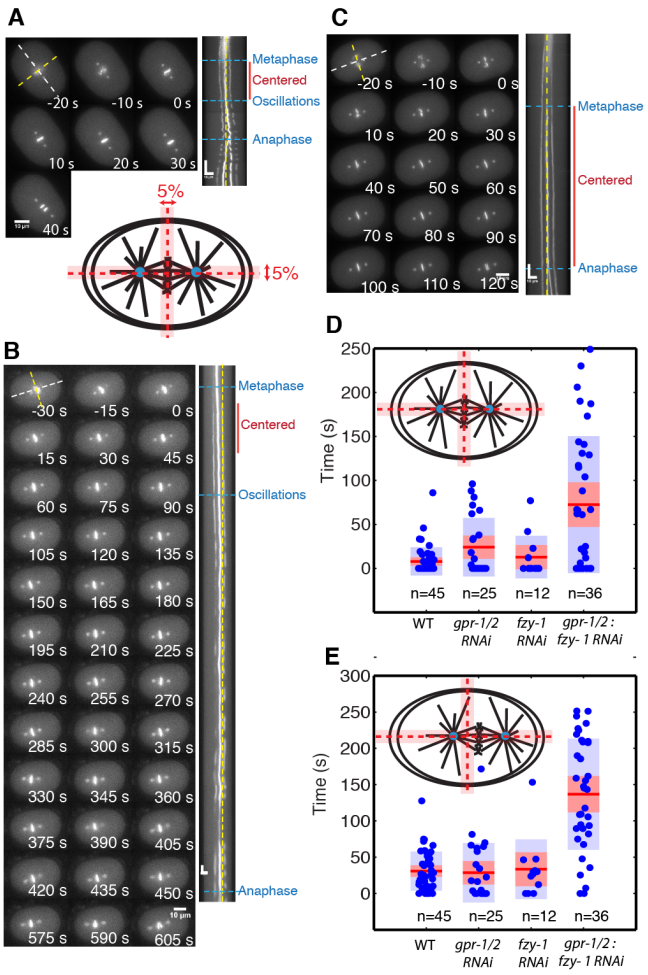

Fig. S9

Spindle centering in *gpr-1/2 (RNAi)* embryos. (A) Mitosis in a control embryo. Left: Images from a time-lapse movie. The A-P axis (white) and the transverse axis (yellow) are depicted in the first image. The formation of the metaphase plate defines $t = 0$. Right: Kymograph (10 fps) along the A-P axis of the embryo shown on the left. Notice that oscillation can begin during metaphase (i.e. before anaphase onset). Lower diagram: Definition of a centered spindle (see methods). **(B)** Mitosis in a *fzy-1 (RNAi)* embryo. Because oscillations begin during metaphase, the centering time remains similar when the embryo was arrested in metaphase (see D and E). **(C)** Mitosis in a *fzy-1:gpr-1/2 (RNAi)* embryo. Because oscillations and posterior movement are both suppressed in this double RNAi, the spindle remains at the cell center for a longer period of time (see D and E). **(D)** Time in which the spindle remained centered in both axis for control embryos, *gpr-1/2(RNAi), fzy-1 (RNAi)* and *gpr-1/2:fzy-1(RNAi)*. The red line denotes the mean, the blue stripe shows the standard deviation and the red stripe shows the 95% confidence interval. For control embryos, the mean time centered was 7.8 ± 2.4 s (mean ± SE). **(E)** Time in which the spindle remained centered only along the A-P axis for control embryos, *gpr-1/2(RNAi), fzy-1 (RNAi)* and *gpr-1/2:fzy-1(RNAi)*. For control embryos this time was 30.1 ± 4.0 s compared to 137 ± 13 s for the double RNAi (*gpr-1/2 and fzy-1)*. Scale bars are 10 μm and 10 seconds.

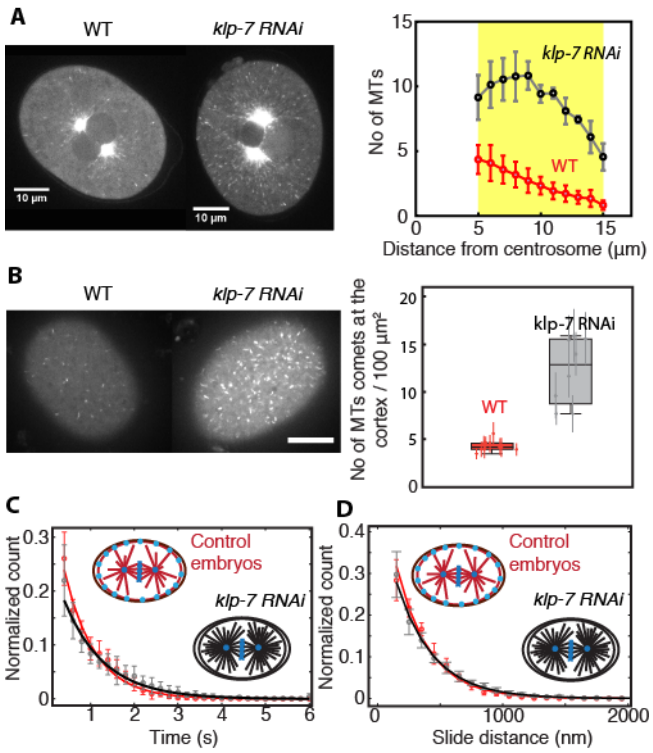

Fig. S10

Microtubule dynamics of *klp-7 (RNAi)* embryos (A) The number of microtubules nucleating from the centrosomes during metaphase in *klp-7 (RNAi)* embryos is higher than in control embryos. Left: Maximum projection images over 1 s of EB-1 comets nucleating from the centrosome in control and *klp-7 (RNAi)* embryos during metaphase. Right: Number of EB-1 comets at varius distances from the centrosome in control (n = 10) and *klp-7 (RNAi)* (n = 2) embryos. **(B)** The number of growing microtubules ends at the cortex during metaphase is higher in *klp-7 (RNAi)* embryos than in control embryos. Left: Maximum projection images over 1 s of EB-1 comets in control and *klp-7 (RNAi)* embryos at the cortex. Right: Number of EB-1 comets at the cortex per 100 µm^2 in control (4.3 ± 0.6, mean ± SD, n = 10, red) and *klp-7 (RNAi)* (12.2 ± 3.5, mean ± SD, n = 8) embryos. **(C)** Distribution of residency times of microtubule ends at the cortex in control (τ = 0.7 ± 0.1 s, n = 10, red) and *klp-7 (RNAi)* (τ = 0.9 ± 0.1 s, n = 8. black) embryos**. (D)** Distribution of sliding distances of microtubule ends at the cortex in control (260 ± 24 nm, red) and *klp-7 (RNAi)* (293 ±11 nm, black) embryos. Error bars are SEs.

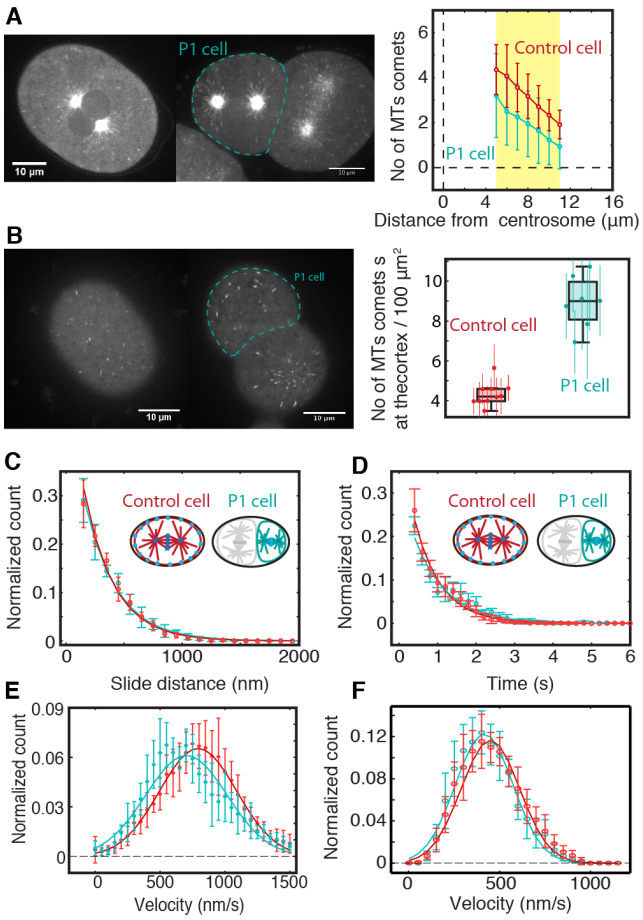

Fig. S11

Microtubule dynamics in the P1 cell. (A). The number of microtubules nucleating from the centrosomes in the P1 cells is approximately 77% that of the control embryos. Left: EB-1 comets nucleating form the centrosome in control and P1 cells. Maximum projection over 1 s. Right: average number of EB-1 comets nucleating from the centrosome to the cortex in the cytoplasm in control cell (n = 10) and P1 cells (n = 8). **(B)** Left: EB-1 comets of in control and in P1 cells. Maximum projection over 1s. Right: boxplot of EB-1 comets at the cortex of embryos during metaphase of control embryos (n = 10) and P1 cells (n = 8). **(C)** Distribution of the residency times of microtubule ends at the cortex during metaphase (τ = 0.7 ± 0.1 s, n = 10, red) and anaphase (τ = 0.8 ± 0.1 s, n = 8, green). **(D)** Distribution of the sliding distances of microtubule ends at the cortex in control cells (260 ± 24 nm, red) and P1 cells (279 ± 19 nm, green). **(E)** Distribution of velocities of microtubule ends in the cytoplasm (see panel A) in control cells (793 ± 9 nm/s, red) and P1 cells (703 ± 30 nm/s, green). **(F)** Distribution of velocities of microtubule ends at the cortex (see panel B) in control cells (448 ± 18 nm/s, red) and P1 cells (414 ± 16 nm/s, green). Error bars are SEs**.**

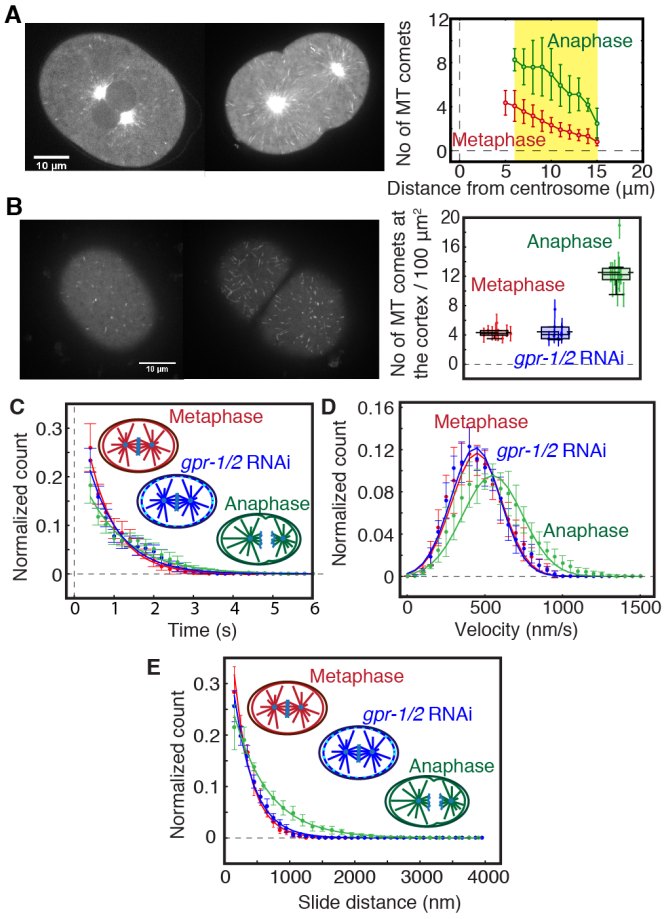

Fig. S12

Microtubule dynamics during anaphase and *gpr-1/2* (RNAi). (A) The number of microtubules nucleating from the centrosomes during anaphase is 2.8 times that in control embryos. Left: EB-1 comets nucleating from the centrosomes in *C. elegans* embryos during metaphase and anaphase. Maximum projection over 1 s. Right: average number of EB-1 comets moving from the centrosome to the cortex in the cytoplasm. **(B)** Left: EB-1 comets of embryos during metaphase and anaphase at the cortex. Maximum projection over 1 s. Right: boxplot of EB-1 comets at the cortex of embryos during metaphase (n = 10), anaphase (n = 10) and *gpr-1/2* RNAi during metaphase (n=10). **(C)** Distribution of the residency times of microtubule ends at the cortex during metaphase (τ = 0.7 ± 0.1 s, mean ± SE, n = 10, red), anaphase (τ = 1.3± 0.9 s, n = 10, green) and *gpr-1/2* RNAi during metaphase (τ = 0.8 ± 0.1 s, n = 10, blue). Single traces display the mean (dots) and the SE (error bars)**. (D)** Distribution of sliding distances of microtubule ends at the cortex in embryos during metaphase (260 ± 24 nm, red), during anaphase (533 ± 24 nm, green) and *gpr-1/2 (RNAi)* embryos during metaphase (303 ± 23 nm, blue). **(E)** Average velocity of microtubules tips at the cortex when sliding along the cortex during metaphase (454 ± 53 nm/s, red), during anaphase (550 ± 67 nm/s, green), and *gpr-1/2 (RNAi)* embryos during metaphase (453 ± 52 nm/s, blue).

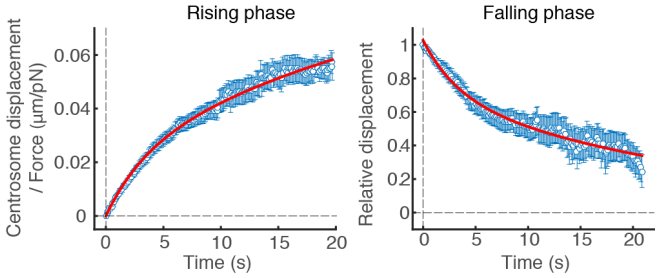

Fig. S13

Average rising and falling phase of the centrosome fit by a simultaneous double exponential. Open blue circles show the average behavior. The error bars are SEs. The solid red curve shows the fit to a double exponential. The red solid lines show the simultaneous double exponential fit (τ_1 = 3.2 ± 0.6 s and τ_2 = 28.4 ± 2.8 s, mean ± 95% confidence interval from non-linear squared fit).

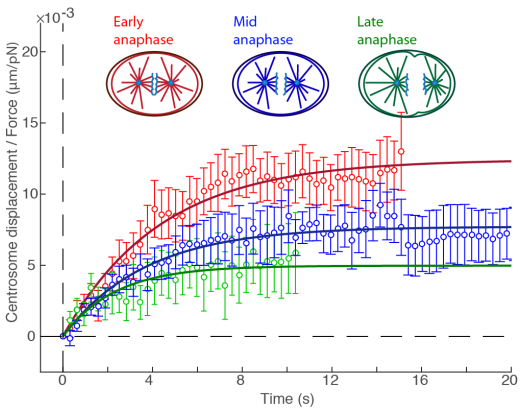

Fig. S14: centering stiffness of *gpr-1/2* (RNAi) embryos during anaphase. Mean rising behavior of spindles during anaphase: early anaphase (0-30 seconds after chromosome separation, red), mid anaphase (blue) and late anaphase (when cytokinesis was evident, green). Solid lines are fits to a Voigt element (Table S2). Error bars are SEs.

Table S1.

E. Coli RNAi strains		
Gene Name	Sequence ID	Library
gpr-1/2	F22B7.13	Ahringer
klp-7	K11D9.1a	Ahringer
fzy-1	F22B5.7	Ahringer

Table S2.

	Group	*n*	Stiffness (κ, pN/μm)			Drag (γ, pNs/μm)			τ (s)		
Anaphase	***gpr-1/2* (all)**	27	119.4	±	21	389	±	81	3.3	±	0.9
	***gpr-1/2* (early)**	11	76	±	17	369	±	116	4.9	±	1.9
	***gpr-1/2* (mid)**	10	126.4	±	28.5	493	±	122	3.9	±	1.3
	***gpr-1/2* (late)**	6	253		[110.1 - 437.2]*	306		[105 - 674]*	1.2		[0.3 – 3.3] *

Error bars are SEs.

* Values in brackets are 95% confidence intervals for asymmetric bootstrap distributions.

Movie S1
Measurement of spindle maintenance forces using magnetic tweezers during metaphase in a single-cell *C. elegans* embryo. Three force pulses were applied to the anterior centrosome using a 1.0 μm bead. In the presence of force, the centrosome moved away from the AP axis and the spindle pivoted around the posterior centrosome. The force pulses had a duration of 10 s except for the last one during which the bead escaped the microtubule array. For more details see Fig. 1 legend.

Movie S2
Rising and relaxation phases of a bead in the cytoplasm. A 1.0 μm bead moved in response to force pulses in the anterior region of a *C. elegans* embryo. The nuclear-centrosome complex was in the posterior region of the embryo. The tracking of the rising and relaxation phases are plotted in the Fig. S7A.

Movie S3
Measurement of spindle maintenance forces using magnetic tweezers during metaphase in the P1 cell of the two-cell *C. elegans* embryo. A single pulse was applied to one of the spindle poles using a 1.0 μm bead. For more details see Fig. S5.

Movie S4
Measurement of spindle maintenance forces using magnetic tweezers during anaphase in single-cell *C. elegans* embryo. Two force pulses were applied to one of the spindle poles using a 1.0 μm bead. For more details see Fig. S5.

Movie S5
Measurement of spindle maintenance forces using magnetic tweezers during metaphase in a single-cell *gpr-1/2:fzy-1 RNAi C. elegans* embryo. A force pulse was applied to the anterior centrosome using a 1.0 μm bead. The magnitude of the force is only shown when the bead makes contact with the spindle pole. The tracking of the centrosome movement is depicted in Fig S6C.